

Structure and Infrastructure Engineering



Maintenance, Management, Life-Cycle Design and Performance

ISSN: (Print) (Online) Journal homepage: https://www.tandfonline.com/loi/nsie20

Seismic fragility analysis using nonlinear autoregressive neural networks with exogenous input

Imran A. Sheikh, Omid Khandel, Mohamed Soliman, Jennifer S. Haase & Priyank Jaiswal

To cite this article: Imran A. Sheikh, Omid Khandel, Mohamed Soliman, Jennifer S. Haase & Priyank Jaiswal (2021): Seismic fragility analysis using nonlinear autoregressive neural networks with exogenous input, Structure and Infrastructure Engineering, DOI: 10.1080/15732479.2021.1894184

To link to this article: https://doi.org/10.1080/15732479.2021.1894184

	Published online: 16 Mar 2021.
	Submit your article to this journal $oldsymbol{arGamma}$
ılıl	Article views: 161
α	View related articles 🗹
CrossMark	View Crossmark data 🗗





Seismic fragility analysis using nonlinear autoregressive neural networks with exogenous input

Imran A. Sheikh^a, Omid Khandel^a (D), Mohamed Soliman^a (D), Jennifer S. Haase^b and Privank Jaiswal^c

^aSchool of Civil and Environmental Engineering, Oklahoma State University, Stillwater, OK, USA; ^bScripps Institution of Oceanography, University of California San Diego, La Jolla, CA, USA; Boone Pickens School of Geology, Oklahoma State University, Stillwater, OK, USA

ARSTRACT

Rapidly growing societal needs in urban areas are increasing the demand for tall buildings with complex structural systems. Many of these buildings are located in areas characterized by high seismicity. Quantifying the seismic resilience of these buildings requires comprehensive fragility assessment that integrates iterative nonlinear dynamic analysis (NDA). Under these circumstances, traditional finite element (FE) analysis may become impractical due to its high computational cost. Soft-computing methods can be applied in the domain of NDA to reduce the computational cost of seismic fragility analysis. This study presents a framework that employs nonlinear autoregressive neural networks with exogenous input (NARX) in fragility analysis of multi-story buildings. The framework uses structural health monitoring data to calibrate a nonlinear FE model. The model is employed to generate the training dataset for NARX neural networks with ground acceleration and displacement time histories as the input and output of the network, respectively. The trained NARX networks are then used to perform incremental dynamic analysis (IDA) for a suite of ground motions. Fragility analysis is next conducted based on the results of the IDA obtained from the trained NARX network. The framework is illustrated on a twelve-story reinforced concrete building located at Oklahoma State University, Stillwater campus.

ARTICLE HISTORY

Received 24 September 2020 Revised 17 December 2020 Accepted 15 January 2021

KEYWORDS

Seismic fragility; neural networks; nonlinear autoregressive neural networks with exogenous input; nonlinear dynamic analysis; incremental dynamic analysis; finite element analysis; structural health monitoring

1. Introduction

The need to improve the resilience and sustainability of building infrastructure in active seismic zones and in other areas at significant risk due to the recent increase in induced seismic hazards has been increasing in recent years (Ellsworth, 2013; Sarkisian, Mathias, Garai, & Horiuchi, 2017). This demand requires structural engineers to design innovative and sometimes very complex structural systems to enhance the performance of new buildings under earthquake hazards. The dynamic response of these structures becomes highly intricate because of the significant contribution of higher modes (Rajbhandari, Anwar, & Najam, 2017). These complexities add to the challenges of accurately predicting the behaviour of these structures and the associated seismic demands (Zain, Anwar, Najam, & Mehmood, 2017). In such situations, the most desired analysis procedure is the nonlinear dynamic analysis. Very often, especially during the preliminary design phase, structural engineers are interested in quantifying a specific performance measure of the structure under different loading scenarios (Rajbhandari et al., 2017). These performance measures include, for example, the maximum drift ratio or the ductile and nonductile component strength based on material behaviour under various earthquake motions corresponding to different hazard levels (Moehle, 2005). In these situations, the iterative execution of full nonlinear dynamic analyses becomes necessary.

Over the past few years, several locations within the central United States have experienced a significant increase in earthquake activity due to induced seismicity (Ellsworth, 2013). Most of the structures in these areas have not been designed to withstand this higher seismicity given the previously low natural earthquake hazard levels in these regions; accordingly, it is necessary to quantify the seismic risk of these vulnerable structures under updated seismic hazard Performance-based earthquake scenarios. engineering (PBEE) (Shokrabadi, Banazadeh, Shokrabadi, & Mellati, 2015) offers robust means for evaluating the seismic risk of structures with complex systems and irregular geometries. When used in conjunction with structural health monitoring (SHM), PBEE can provide a realistic prediction of the dynamic behaviour of the investigated structure. A PBEE framework that helps in quantifying the fragility of the structure, requires proper seismic hazard quantification and response assessment at various hazard levels (Aghayan, Jaiswal, & Siahkoohi, 2016; Lagaros & Papadrakakis, 2012).

Fragility analysis is a method to estimate the probability of a structure reaching or exceeding a certain damage state given a specific hazard intensity (Gidaris et al., 2017). This method, which is a key component of the risk assessment, can be conducted using incremental dynamic analysis (IDA)



(Ibrahim, 2018) that quantifies the structural response under a suite of ground motions with different intensity levels (Vamvatsikos & Cornell, 2002). Hence, the process of developing the fragility curves for a given structure involves conducting numerous nonlinear analyses in order to properly incorporate the underlying uncertainties (Kiani, Camp, & Pezeshk, 2019).

Various finite element (FE) analysis software packages that are currently available can be used for conducting nonlinear dynamic analyses. In general, these packages can predict the seismic demand forces for complex structures with reasonable accuracy (Zhang et al., 2019). However, detailed nonlinear time history analysis (NLTHA) can be computationally very demanding and the computational cost increases significantly for complex structural systems (Lavaei & Lohrasbi, 2012). For instance, Zain et al. (2017) analysed a 55-story building using PERFORM 3 D (CSI, 2020) and reported a computational time of 30 hours to conduct the analysis using a desktop computer with a 3.4 GHz processor and 4.0 GB RAM. Accordingly, risk assessment of complex structures that integrates traditional NLTHA may be deemed unfeasible due to the associated computational cost. In these situations, it is necessary to develop more efficient and robust tools that can predict the nonlinear dynamic response of structures; especially if the long-term objective is to use the response prediction tools in probabilistic risk analysis or near real-time performance prediction and damage assessment.

One approach to reduce this computational burden is to use surrogate models, also known as metamodels (Gidaris, Taflanidis, & Mavroeidis, 2015). Soft computing methods, based on heuristic approaches that exploit the tolerance for imprecision and uncertainty, have been proposed to develop metamodels for various engineering problems. Artificial neural networks (ANNs), genetic algorithms, fuzzy logic, and decision tree analysis are among the popular methods in soft computing (Zain et al., 2017). Owing to their computational efficiency and ability to predict accurate relationship between data points (Alexandridis, 2013), ANNs have been widely used in solving structural engineering problems such as design optimization (e.g. Lagaros, Plevris, & Papadrakakis, 2010; Papadrakakis & Lagaros, 2002), structural reliability analysis (e.g. Hurtado & Alvarez, 2001; Khandel & Soliman, 2021; Lagaros & Fragiadakis, 2007), and damage detection and localization (Khandel, Soliman, Floyd, & Murray, 2020). ANNs have also been used in the field of structural dynamics. For example, they have been implemented in Ok, Son, and Lim (2012) to predict displacement caused by dynamic loading on bridges. Additionally, Masri, Nakamura, Chassiakos, and Caughey (1996) adopted a multi-layer perceptron (MLP) architecture (Pal & Mitra, 1992) to predict the dynamic response of various systems.

In the context of predicting the seismic response of buildings, where nonlinear response at a certain time instant depends upon the previous state of the system (i.e. time series problems), regular neural networks such as MLP architectures suffer inefficiencies due to their simple architecture and require numerous iterations for their training (Patra & Bornand, 2010). Therefore, research is still needed to develop approaches that can accurately predict the dynamic

response of nonlinear structures using ANNs. Recently, Zhang et al. (2019) have implemented deep long short-term memory (LSTM) networks to predict the nonlinear seismic response of structures. However, training LSTM networks for datasets containing long range dependencies becomes difficult since LSTM networks may suffer from the gradient vanishing problem (Arjovsky, Shah, & Bengio, 2016).

This is a particular issue with the networks that utilize the gradient descent learning algorithms and have 'hidden states' in their architecture (Lin, Horne, Tino, & Giles, 1996). In Wu and Jahanshahi (2018), deep convolution neural networks have been applied for system identification and estimation of nonlinear structural dynamic response. However, as demonstrated in Wu and Jahanshahi (2018), deep convolution neural networks require a relatively large training dataset. The need for large training datasets negates the benefits sought after by using metamodels.

To address these limitations, nonlinear autoregressive neural networks with exogenous input (NARX) are used in this paper to predict the response of complex nonlinear dynamic systems. Recently, NARX neural networks have been used in various engineering problems involving modeling of nonlinear systems. Inundation levels during typhoons have been predicted in Ouyang (2017) using both open loop and closed loop NARX neural networks while Ruiz, Cuellar, Calvo-Flores, and Jimenez (2016) predicted energy consumption in buildings using NARX networks. These NARX networks not only use gradient descent learning algorithms that are more efficient than other recurrent networks such as LSTM networks, but they also rely on tapped feedback delays which make them suitable for modeling systems with long range data dependencies (Lin et al., 1996).

Accordingly, this paper adds to existing literature by establishing a framework for seismic fragility analysis of complex structural systems using NARX neural networks. The presented approach integrates neural networks and nonlinear FE analysis to quantify the structural response during seismic excitations. Such approach was found to provide a highly accurate prediction of the structural response during high-intensity seismic events compared to existing methodologies relying on other surrogate models such as feedforward ANNs or LSTM networks. SHM information collected during seismic events is used to calibrate key input parameters of the FE model. NARX neural networks are then trained using the results of nonlinear FE analyses of the structure. The trained NARX networks are used to obtain the critical peak ground accelerations and maximum interstory drift by means of incremental dynamic analysis. These quantities are next used to develop the seismic fragility curve of the investigated building. The framework is illustrated on an existing twelve-story reinforced concrete building in Stillwater, Oklahoma.

2. Seismic fragility analysis

Fragility quantification is a crucial component in seismic risk assessment based on PBEE (Kiani et al., 2019). In addition to its role in risk assessment, fragility analysis is

generally needed for retrofit design and post-disaster decision making and planning (Celik & Ellingwood, 2009). Seismic fragility can be defined as the conditional probability of exceedance of a limit state function given a certain seismic intensity measure. Mathematically, seismic fragility F_r can be expressed as (Zain et al., 2017):

$$F_r = P(LS > l \mid IM = m) \tag{1}$$

where LS represents the limit state function, l being the limit of the function, IM represents the intensity measure, and m denotes a particular value of intensity measure.

Several approaches have been proposed for establishing the fragility curves of structural systems depending upon the processes used to capture the structural response. These approaches can be classified into three broad categories: (a) analytical approaches, which are based on investigating data obtained from structural analyses (Ibarra & Krawinkler, 2005); (b) empirical models, in which the statistical analysis of post-earthquake data is used to establish the exceedance measures (Sabetta, Goretti, & Lucantoni, 1998); and (c) heuristic approaches based expert opinions (Jaiswal, Aspinall, Perkins, Porter, 2012).

To properly quantify the structural fragility, a model capable of representing the realistic nonlinear inelastic behaviour of the system is required. This can be achieved for newly designed structures; however, for existing structures, developing an accurate numerical model may not be a straightforward task. For these structures, modeling difficulties may arise due to the absence of detailed construction drawings, variations between the design and as-built characteristics, and unknown material properties. In addition, depending on the age of the structure, time-dependent deterioration (e.g. corrosion and concrete cracking) or structural damage due to excessive or repetitive loading (e.g. history of significant seismic exposure) may have caused a shift in the structural properties that adds to the challenges in constructing an accurate structural model. In this context, SHM plays a vital role in quantifying the realistic dynamic performance of the investigated structure. During a seismic event, SHM can record the input excitation affecting the structure and the resulting response output.

The structural performance parameters of interest are typically the: (a) accelerations, measured by strong motion accelerometers, (b) rotations, measured in special cases by gyroscopes, and/or (c) precise displacements, measured by Global Positioning System (GPS) receivers, strainmeters, or string potentiometers. By integrating SHM with system identification methods, the optimum values of key model parameters can be achieved resulting in a better representation of the structural behaviour (Sheikh, Khandel, Soliman, Haase, & Jaiswal, 2019). Furthermore, SHM systems assist in detecting changes in the structural properties (Yi et al., 2012) and the occurrence of structural damage (Rainieri, Fabbrocino, & Cosenza, 2011) along the service life of a structure.

Conducting nonlinear dynamic analysis can be achieved either by fast nonlinear analysis (FNA) or direct integration.

FNA, also known as modal time history analysis, is based on modal analysis with a nonlinear force vector. Owing to its computational efficiency, it is widely used in the design community, but it has limited capabilities in accounting for the nonlinear system attributes. On the other hand, the direct integration method is a step-by-step method which allows the inclusion of different nonlinear components within the analysis model (CSI, 2018).

This paper implements the direct integration method to model the nonlinear behaviour using cross-sectional fibres and plastic hinges which cannot be properly considered using the FNA. Mathematically, the direct integration method involves solving the equation of motion:

$$\mathbf{K}u(t) + \mathbf{C}u'(t) + \mathbf{M}u''(t) = F(t)$$
 (2)

in which K represents the stiffness matrix of the system, C represents the damping matrix of the system, M is the mass matrix, F(t) is the force vector, and u(t), u'(t), and u''(t)are the displacement, velocity and acceleration vectors of the system, respectively. In general, FE solvers use numerical approaches such as Newmark's method (Newmark, 1959) or Hilber-Hughes-Taylor method (Hilber, Hughes, & Taylor, 1977) to solve the equation of motion.

Incremental Dynamic Analysis, sometimes referred to as dynamic pushover analysis, is a parametric analysis technique that can be used to develop analytical fragility curves (Ibrahim, 2018). In the IDA, a suite of ground motion time histories, either real or simulated, are selected, scaled progressively, and applied to the nonlinear model of the structure until a specific limit state or failure criterion is achieved (Vamvatsikos & Cornell, 2002). The incremental dynamic analysis results in the IDA curves which provide the relationship between the ground motion, as the intensity measure, and the engineering demand parameter of the structural response (e.g. maximum interstory drift). IDA not only provides a useful engineering insight on the behaviour of a structure, but it offers deeper understanding of the structural response under different intensities ground motion.

Analytical fragility curves can be established from the outcome of the dynamic analysis under multiple excitations using the Log-Normal (LN) cumulative distribution function (CDF). The LN distribution model has been shown to provide accurate representation of the seismic fragility (Ibarra & Krawinkler, 2005; Lallemant, Kiremidjian, & Burton, 2015). Due to the multiplicative reproducibility characteristic of the LN distribution, it has emerged as a powerful tool in the development of reliability and risk metrics (Lallemant et al., 2015). Mathematically, a fragility function, based on LN CDF, is expressed as (Baker, 2015):

$$P(LS|IM = x) = \Phi\left(\frac{\ln(x/M)}{\sigma}\right)$$
 (3)

where Φ represents the standard normal cumulative distribution function (CDF), P(LS|IM = x) is the probability that the ground motion with IM = x will cause the structure to reach the defined damage state LS, M is the median of the fragility function, and σ is logarithmic standard deviation, also referred to as the dispersion of IM.

However, as indicated earlier, conducting several full-scale dynamic analyses may not be computationally feasible, especially when nonlinear behaviour is incorporated in the model. Alternatively, the approach presented in this paper uses soft-computing tools to reduce this computational burden. Herein, a trained NARX neural network will be used to conduct the IDA for developing the fragility curves of the investigated structure.

3. NARX neural network

NARX is a nonlinear, dynamic model that relates two time series, an input/independent time series to an output/ dependent time series (Siegelmann, Horne, & Giles, 1997). It estimates the current value of a time series data with respect to past values of the same series and the current and past values of an exogenous/independent series. In case of approximating the structural response given an earthquake excitation time history, the independent/input or exogenous time series, v, will represent the realization of the earthquake ground acceleration time history, and the dependent/ output time series, u, will represent the output displacement time series of the structural response at each floor. G is the mapping (transformation) function that establishes the relationship between the input and output which will eventually replace the nonlinear FEM model with a computationally efficient approximation. In general, the NARX structure can be mathematically represented as (Lin, Horne, Tino, & Giles, 1996):

$$u(t) = G(u(t-1), u(t-2), ..., u(t-k), v(t), v(t-1), v(t-2), ..., v(t-k))$$
(4)

where k represents the number of feedback and/or input delays (Menezes & Barreto, 2006).

When this nonlinear function *G* is approximated using neural networks, the resulting system is known as NARX neural network (Siegelmann, Horne, & Giles, 1997). A neural network is an algorithm intended to identify numerical patterns in data. A neural network consists of at least three layers; input, hidden, and output layers. The input layer introduces input data to the neural network which is then fed to the hidden layer(s). The output layer is the last layer of a neural network which yields the output of the network (Montana & Davis, 1989).

Apart from these layers, there are two essential components of a neural network; activation functions and model parameters. An activation function accepts an input value and yields an output value by transforming the activation level of a neuron (Sibi, Jones, & Siddarth, 2013). The model parameters are the weights and bias values associated with the connections between the neurons of a network. Mathematically, an activation function for a single neuron i can be represented by a linear combination as (Sibi, Jones, & Siddarth, 2013):

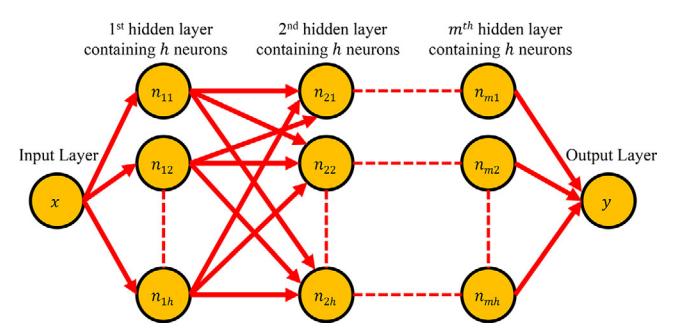


Figure 1. Typical configuration of a neural network.

$$y_i(t) = g\left(\sum_{j=1}^{n_j} w_{ij}(t) * x_j(t) + b_i(t)\right)$$
 (5)

where $x_j(t)$ represents the input value of parameter j at time t, $y_i(t)$ represents the output quantities at neuron i and time t, g denotes the nonlinear activation function, n_j is the number of parameters, $w_{ij}(t)$ is the weight assigned by neuron i to the input value of parameter j at time t, and $b_i(t)$ represents the bias value at neuron i and time t.

These weights and bias values are adjusted during the training phase of the neural network which results in the estimation of the mapping function *G*. Hence, training a neural network is establishing the optimum values of these weights and bias values. A network training function is used to update these model parameters by evaluating a cost function such that the difference between the predicted values obtained by the network and the target values is minimum (Wang, Pedroni, Zentner, & Zio, 2018). The mean squared error (MSE) is one of the commonly used cost functions and is computed as (Joghataie & Farrokh, 2008):

$$MSE = \frac{1}{n_t} \sum_{i=1}^{n_t} \left(u_{network} - u_{target} \right)^2$$
 (6)

where $u_{network}$ is the value predicted by the neural network, u_{target} is the target value, and n_t is the number of time points in a given input. Figure 1 presents a configuration of a typical neural network. The depicted neural network architecture contains one input, one output and m hidden layers. Each hidden layer includes h neurons. The arrows connecting the neurons pass the predicted output and the assigned weight and bias values associated with each neuron to the next layer.

NARX is a type of neural network that can be implemented in both feedforward and recurrent network configurations. A feedforward network consists of a series of layers where input layer and output layer sandwich the hidden layer(s) (Mathworks, 2019). There are no closed loops in this network configuration, hence no feedback, and the data flows in one direction. However, in a recurrent neural network, there are closed loops which provide feedback in the form of output data to the input of neural network again (Ouyang, 2017). NARX neural networks have been shown to be very efficient compared to ordinary neural networks; hence, these networks are known to be equivalent to Turing machines (Menezes et al., 2006).

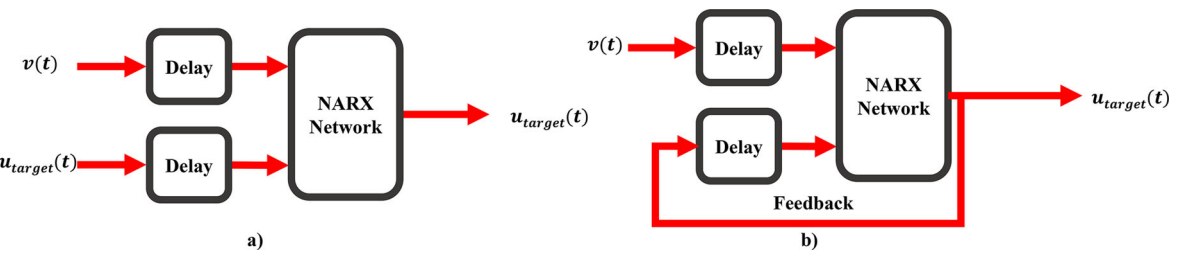


Figure 2. Configuration of NARX neural network: (a) open loop, (b) closed loop.

A NARX neural network can be used in both architectures: open loop (or series-parallel) and closed loop (or parallel) as shown in Figure 2. In open loop, both time series are given as input to the model, while in the closed loop architecture, the NARX predicts the value of the dependent series and then feeds the predicted values up to that time point back into the model in place of the known target time series (Ouyang, 2017). In this paper, the open loop configuration is used for training the neural network while the closed loop configuration is used for the validation and prediction. For training, the seismic excitation signal (i.e. v(t)) and the corresponding structural response (i.e. u_{target}) are used as input time series, while for testing, the network uses only the seismic excitation to predict the structural response (i.e. $u_{network}$).

In this paper, NARX networks are used within an integrated framework for quantifying the seismic fragility of multistory buildings. The layout of the framework is shown in Figure 3. The framework starts with constructing the finite element model of the investigated structure. In this phase, a nonlinear structural model is required to represent the realistic behaviour of the structure during seismic events. SHM data is integrated to calibrate the structural model. A suite of ground motion records is selected based on magnitude and source to site distance. The calibrated FE model is then used to conduct nonlinear dynamic analyses to generate the training and testing datasets for the NARX neural networks. The dataset is next used to train and validate the NARX neural networks. Once trained, the NARX networks are used to conduct the IDA considering peak ground acceleration (PGA) as the intensity measure and maximum interstory drift ratio (IDR) as the engineering demand parameter. Seismic fragility curves are then developed based on the generated IDA curves.

Note that the presented framework can be used for design and assessment of new or existing structures. SHM data may not be available in the design phase of new buildings; additionally, SHM data collection may be expensive or not feasible for existing systems. Accordingly, the framework is designed with the FE model calibration as an optional step. In summary, if SHM data is unavailable, the FE model can still be directly integrated into the framework to establish the training and testing dataset for the NARX network.

4. Illustrative example

The presented framework for fragility analysis using NARX neural networks is illustrated on a twelve-story reinforced

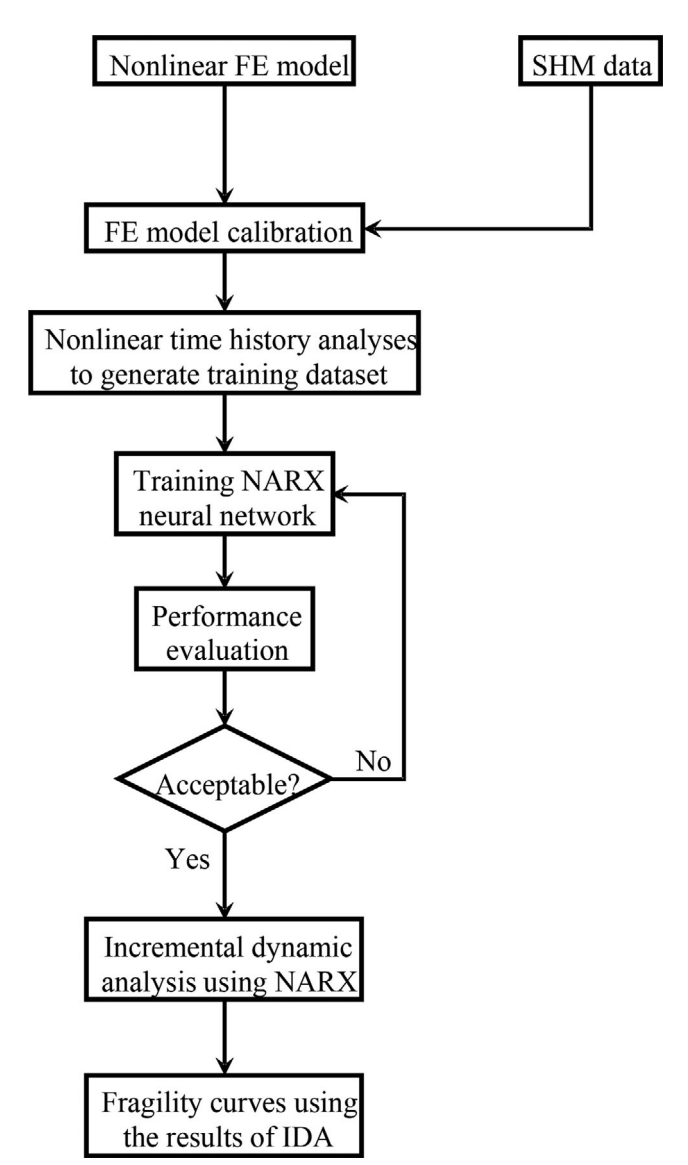


Figure 3. Layout of the proposed framework for conducting fragility analysis using NARX neural networks.

concrete building located on the campus of Oklahoma State University, Stillwater. The selected building, Kerr hall, is a residential building constructed in the 1960s. The building is 57m (187.5 ft) long and 16.8 m (55.3 ft) wide with a total height of 36.7 m (122.3 ft). The height of first story is 3.7 m (12.3 ft) while the rest of the stories are 3 m (10 ft) high. The lateral load resisting system consists of moment frames and shear walls while the gravity load system consists of reinforced concrete slabs and gravity columns.

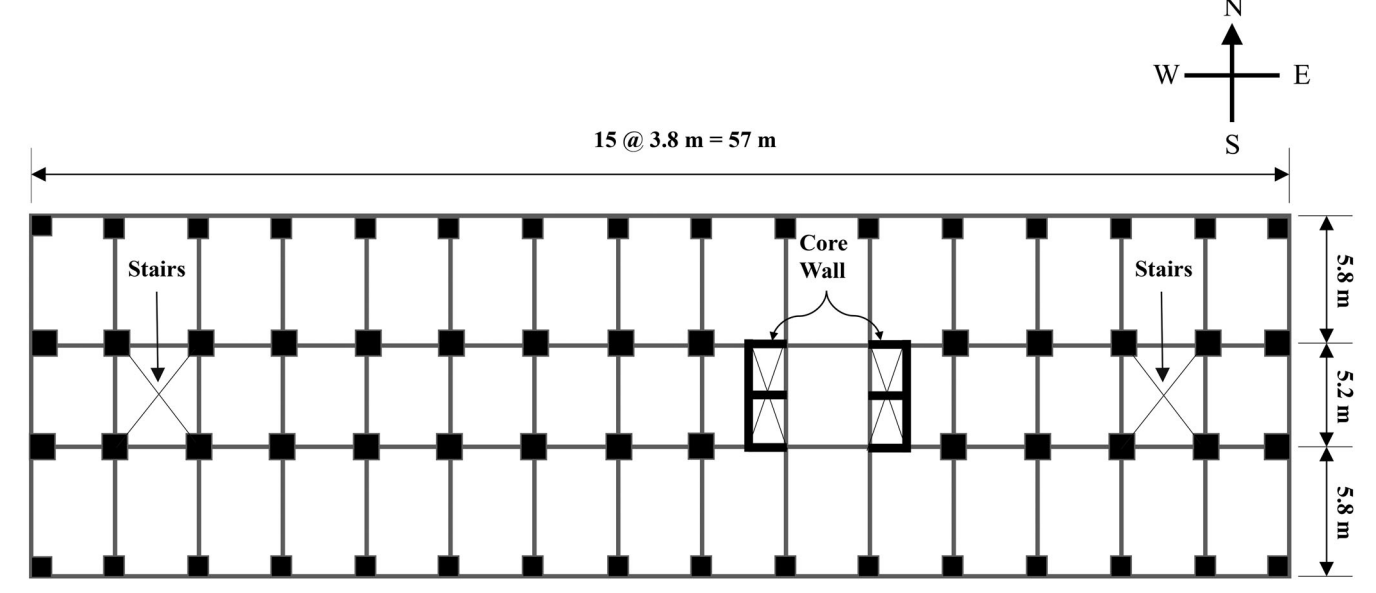


Figure 4. Plan view of the investigated building.



Figure 5. GPS antenna mounted on the roof.

The building has two staircases and two shear wall cores that house the elevators. Figure 4 shows the plan view of the investigated building. Given the increase in the seismic activity in the region, the building was instrumented to assess its acceleration response, rotations and displacements during seismic events. A GPS antenna, shown in Figure 5, was installed on the roof level of the building to measure the realtime displacements during an earthquake. The difference between the GPS positions before and after an earthquake can provide the residual deformations. Two triaxial strong motion accelerometers, one at the ground level and one at the roof, were mounted to record the ground acceleration and building response during an earthquake. Similarly, two triaxial gyroscopes were installed to capture the rotational behaviour of the building during seismic events. Figure 6 depicts the installed accelerometer and gyroscope.

On April 07, 2018, an earthquake of magnitude 4.6 struck northern Oklahoma. The epicentre was located at approximately 47 km from the investigated building at a depth of 10 km. At the time of the earthquake, only the triaxial accelerometers and the GPS were fully functional. However, because the earthquake was not large enough to generate displacements above the GPS noise level, only the acceleration time

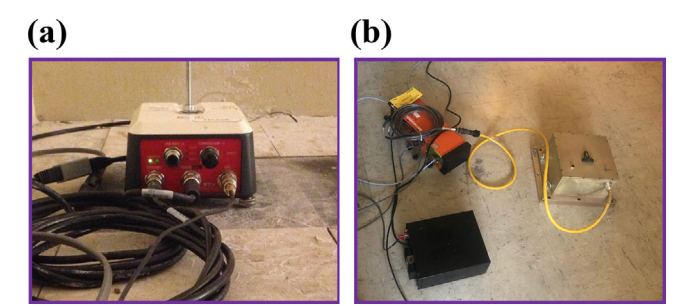


Figure 6. Instrumentation installed in the building (a) accelerometer and (b) gyroscope.

histories recorded during this earthquake will be used herein to calibrate the finite element model of the building.

4.1. Finite element modelling

A three-dimensional finite element model of the building, as shown in Figure 7, is created in CSi SAP2000 environment (CSI, 2018) based on the as-built structural drawings provided by the university administration. Nonlinearity in the model is introduced at both the material and geometric levels. Reinforced concrete is modelled using Mander's concrete model (Mander, Priestley, & Park, 1988) as an isotropic material with cylinder compressive strength of 34.5 MPa (5,000 psi) for columns and shear walls, and 27.6 MPa (4,000 psi) for all other members.

Figure 8 displays the stress-strain curve for 34.5 MPa (5,000 psi) concrete used in this analysis. A parametric stress-strain model which takes into account the strain hardening behaviour (CSI, 2018) is used for the steel reinforcement. The stress-strain profile for the adopted parametric model is given as:

$$\sigma = \begin{cases} \varepsilon & \text{for } \varepsilon < \varepsilon_y \\ \sigma_y & \text{for } \varepsilon_y < \varepsilon < \varepsilon_{sh} \\ \sigma_y + (\sigma_u - \sigma_y) \sqrt{\frac{\varepsilon - \varepsilon_{sh}}{\varepsilon_u - \varepsilon_{sh}}} & \text{for } \varepsilon > \varepsilon_{sh} \end{cases}$$
(7)

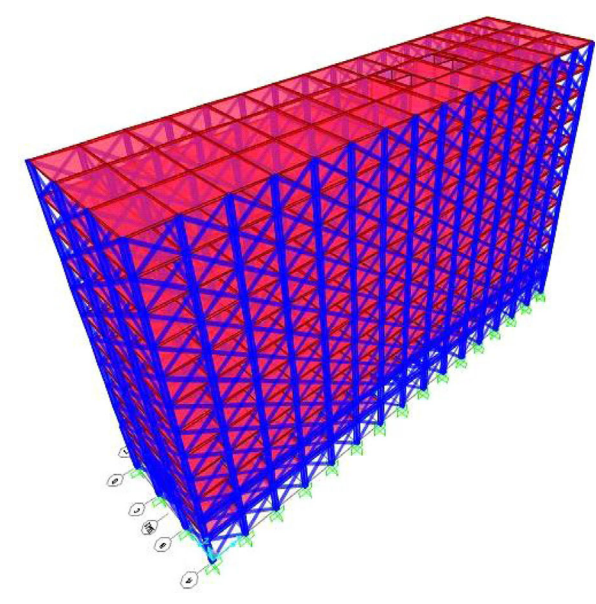


Figure 7. Finite element model of the building in CSi SAP2000.

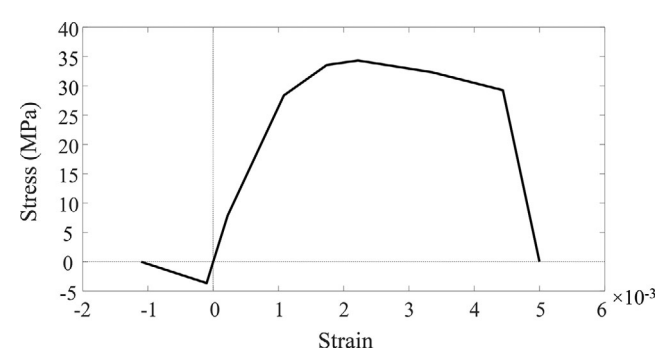


Figure 8. Stress-strain curve of the 34.5 MPA (5,000 psi) concrete using Mander's model.

in which σ is the rebar stress, E is the modulus of elasticity, ε is the rebar strain, σ_v represents the yield stress, σ_u is the ultimate stress, ε_v is the yield strain, ε_{sh} is the strain at the onset of strain hardening, and ε_u is the ultimate strain. Figure 9 shows the stress-strain profile for the steel reinforcement with yield strength of 345 MPa (50 ksi) used in this model.

Fibre modelling is adopted to properly account for the inelastic sectional behaviour of columns. This technique allows the inclusion of plasticity distribution along the member and across its section (Celik & Ellingwood, 2009; Salihovic & Ademovic, 2017). In the fibre modelling approach, the cross-section of the column is divided into small axial fibres. Depending upon the material, whether steel or concrete, each fibre is assigned its own nonlinear stress-strain curve. This process allows capturing the axial force and moment interaction in the elements, as well as the effects of cracking and yielding across and along the member (PEER/ATC-72, 2010). Integrating the resultant behaviour on the cross-section level along the length using the aforementioned material constitutive laws provides the required force-deformation relationships. This approach is not only suitable for quantifying the nonlinear inelastic response under dynamic loading, but it also provides a

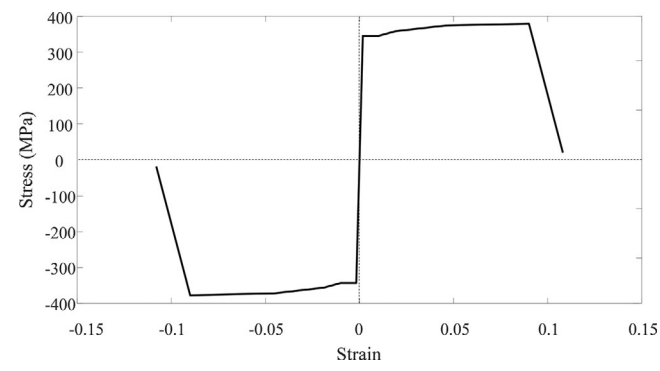


Figure 9. Parametric stress-strain relationship for steel reinforcement with yield

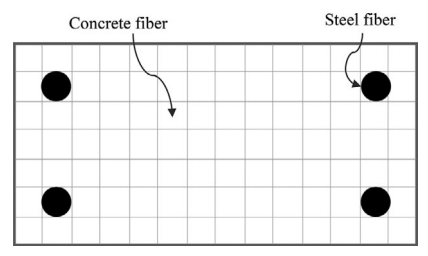


Figure 10. Typical cross-section as implemented in the fiber modeling approach.

reliable and efficient solution (Lagaros & Papadrakakis, 2012). Figure 10 depicts a schematic representation of fibre modelling approach.

Plastic hinges are assigned to the ends of the beams to model the nonlinear frame behaviour as lumped plasticity. Plastic hinge modelling has been shown to properly represent the building behaviour near collapse loading conditions and also allows capturing the concrete crushing and rebar buckling behaviour in the model (Shokrabadi et al., 2015). Simulating the nonlinear behaviour of plastic hinges was achieved by defining a backbone curve as opposed to fibre modelling where each fibre is assigned a full nonlinear stress-strain curve. The backbone curve parameters (i.e. plastic rotation angle and residual strength ratio) are selected herein based on FEMA 356 (FEMA, 2000). A plastic hinge backbone curve is shown in Figure 11 where 'a', 'b', and 'c' are parameters that depend on the material properties, cross-sectional dimensions, and reinforcement ratio.

The hysteretic behaviour is incorporated in this example using Takeda's stiffness degrading model (Takeda, Sozen, & Nielsen, 1970). This model was shown to represent the realistic behaviour of reinforced concrete systems under dynamic loading. It takes into account the change in stiffness associated with flexural cracking and yielding of reinforcement in addition to incorporating the strain-hardening effects (Otani, 1980). In this model, the unloading curve follows the elastic portion of the backbone curve and the reloading curve follows a secant line. If the applied load exceeds the yield load, the unloading curve follows an exponential function (Takeda, Sozen, & Nielsen, 1970). However, this exponential unloading behaviour is considered linear herein due to software limitations. The maximum deformation point in the previous cycle becomes the target point

for the secant line in next cycle. As a result, the hysteresis loop continues to reflect the reduction in energy dissipation with increased deformation levels. Since hysteretic damping is already considered within the hysteresis behaviour, Rayleigh damping of 4% is used to account for viscous damping as opposed to the traditionally adopted 5% (PEER/ ATC-72, 2010). Second-order nonlinear behaviour is also incorporated explicitly in the model.

Being a residential hall, the building consists of a large number of infill walls that may have a significant influence on the stiffness of the structure. The stiffness contribution of infill walls is included in the model using equivalent diagonal compression-only struts following FEMA 356 recommendations (FEMA, 2000). The strut thickness is chosen equal to the thickness of the walls while the width of the strut a is calculated as (FEMA, 2000):

$$a = 0.175 \ (\lambda_1 h_{col})^{-0.4} r_{inf} \tag{8}$$

in which:

$$\lambda_1 = \left[\frac{E_{me} t_{inf} \sin 2\theta}{4 E_{fe} I_{col} h_{inf}} \right]^{\frac{1}{4}} \tag{9}$$

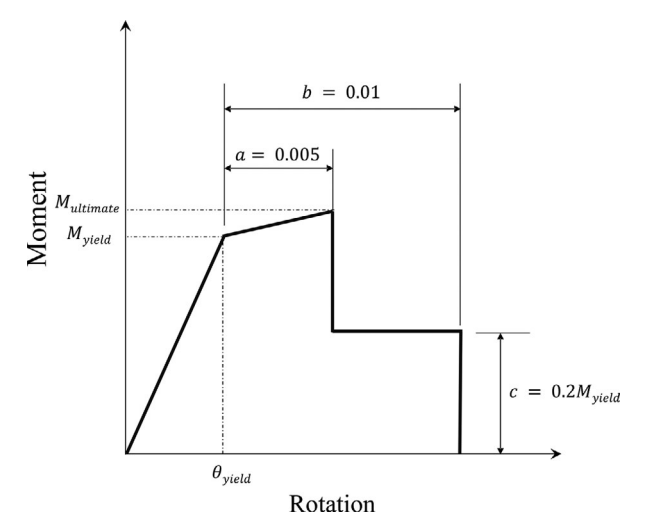


Figure 11. Backbone curve for the plastic hinge using FEMA 356.

where t_{inf} is the thickness of infill wall and strut, L_{inf} is the length of infill wall, r_{inf} represents the diagonal length of infill wall, I_{col} is the second moment of area of column, E_{me} is the expected elastic modulus of infill wall, E_{fe} is expected elastic modulus of frame, and θ represents the angle whose tangent is the infill height-to-length ratio. As shown in Figure 12, h_{inf} represents the height of infill wall and h_{col} is the height of column. The behaviour of all floor slabs is assumed elastic and they are modelled as thin shell elements where transverse shear deformations are neglected. Rigid diaphragms are assigned to each story level to model the inplane stiffness.

4.2. FE model calibration

To improve the ability of the FE model to represent the analysed structure, SHM information is used to calibrate the structural model. The ground acceleration recorded during the April 07, 2018 earthquake is applied to the finite element model and the corresponding recorded roof acceleration is compared to the time history resulting from the FE model under the same excitation.

Bending stiffness values of the columns along both axes are chosen as the calibration parameters. Optimum values of these parameters are determined such that the difference between the modal frequencies obtained from SHM data analysis and the finite element model is minimized. For this optimization, the objective function is defined as:

$$e(\mathbf{X}) = \sum_{i=1}^{n} W_i. \left(\frac{f_{co,i}(\mathbf{X}) - f_{o,i}(\mathbf{X})}{f_{o,i}(\mathbf{X})} \right)^2$$
(10)

where $e(\mathbf{X})$ is the objective function, $f_{co,i}(\mathbf{X})$ is the computed natural frequency of mode i using finite element analysis, $f_{o,i}(\mathbf{X})$ is the observed natural frequency of mode i using SHM data analysis, W_i is the weighting factor of mode i, n is the number of considered vibration modes, and X is the vector of calibration parameters (i.e. bending stiffness for columns). This optimization problem is solved using a sequential quadratic programming algorithm to establish the optimum values of the column stiffness. The

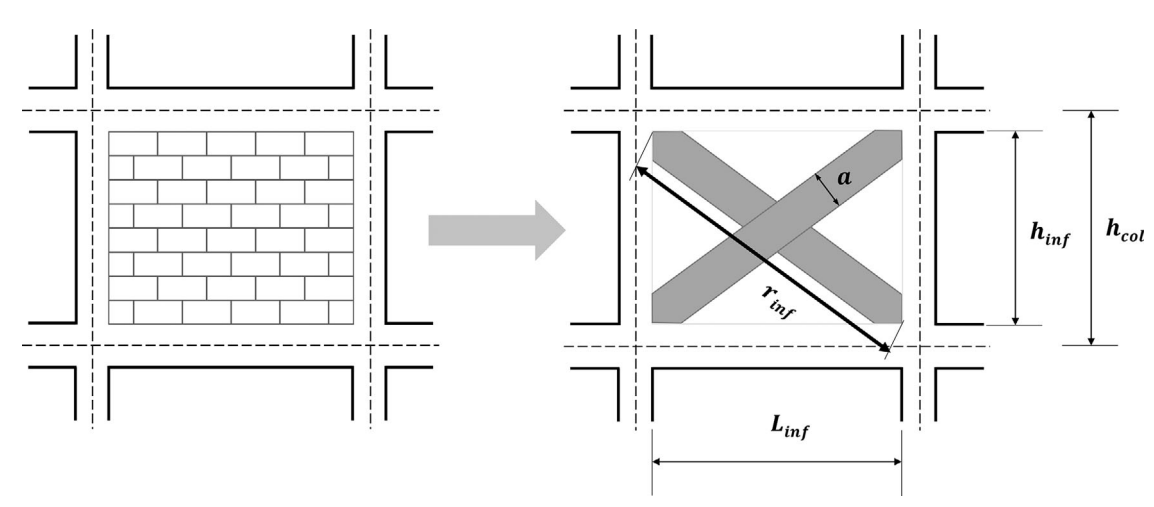


Figure 12. Equivalent diagonal compression strut model using FEMA 356.

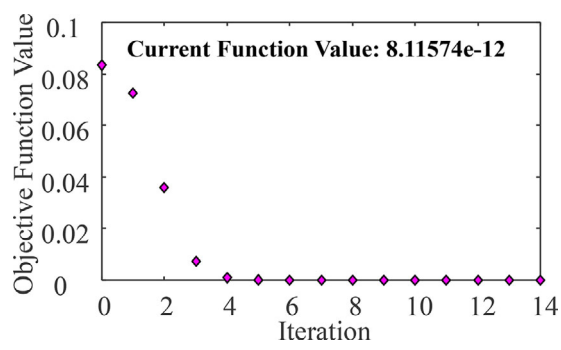


Figure 13. Convergence of the FE calibration optimization.

first three natural modes of the building, which cover almost 90% of the modal mass participation, are considered for model calibration. These modes are assumed to be equally important with weighting factors equal to one. Figure 13 depicts the convergence plot for the FE calibration optimization. As shown, the value of the objective function reaches the minimum value after 14 iterations.

Figures 14 and 15 illustrate the roof-to-base power spectral density (PSD) ratio for the SHM recorded response and calibrated FE model in both directions. As shown, the FE model is capable of representing the structural behaviour. The power spectral ratio of FE model and actual structure are close in both low and high frequency ranges. However, a variation between some of the SHM-based and FE-simulated peak amplitudes can be observed. This variation can be attributed to the complex damping behavior of the structure.

Figure 16 displays the probability plot of the frequencies at which peaks occur in the roof-to-base PSD ratio plots obtained from SHM data and the FE model. As shown, the FE model reports the peak values to occur at almost the same frequencies at which the SHM data exhibit peaks; especially in lower frequencies that have higher contribution to the system response. Figure 17 depicts the structural health monitoring acceleration time series recorded at the rooftop for the April 07, 2018 earthquake and the response generated by the FEM model. As can be seen from this figure, the FE model is capable of predicting the dynamic response of the building under seismic excitations, closely matching the amplitude of shaking following the shear wave. Figure 17(b) illustrates the realistic reproduction of the predominant frequencies at 2 Hz and 12–13 Hz.

4.3. Neural network training

Ideally, a set of historically recorded ground motion records at the region of interest should be used for performing IDA analysis. Each of these records is then scaled to cover multiple levels of seismic intensities to force the structure through its entire behaviour spectrum. However, the structure investigated herein is located in Stillwater, Oklahoma, which recently started to experience high seismic activity induced by oil and gas production (McNamara et al., 2015).

Consequently, the limited earthquake acceleration records available for the region are not sufficient for conducting the

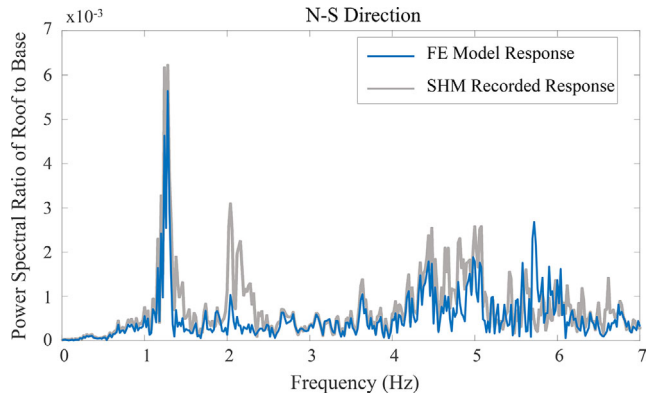


Figure 14. Comparison of PSD ratio (N-S direction).

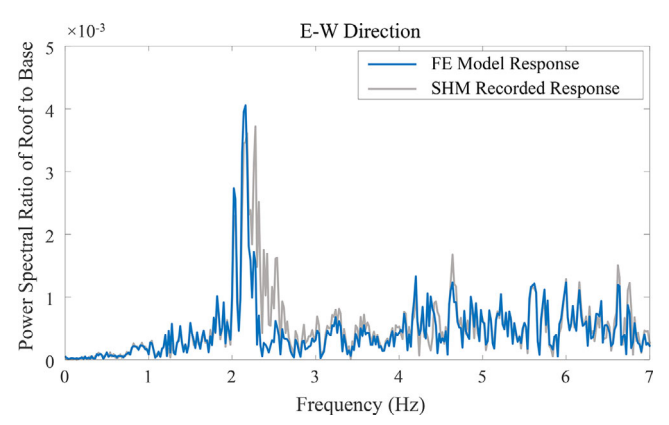


Figure 15. Comparison of PSD ratio (E-W direction).

IDA analysis and fragility assessment. Accordingly, ground motion records of real earthquakes are obtained from the Next Generation Attenuation (NGA-West2) database created by the Pacific Earthquake Engineering Research (PEER) centre (PEER, 2008). The selected earthquake records have magnitude range of 4.0–7.5 and Joyner-Boore (Joyner & Boore, 1981) distance R_{JB} (PEER, 2008) of less than 100 km. The selected acceleration time histories are then used in the finite element analysis to generate the training dataset for the NARX neural networks.

These earthquake signals cover the expected PGA range needed for conducting the IDA and fragility analysis. They also exceed the intensity level expected to occur at the building location based on the probabilistic hazard assessment conducted in Petersen et al. (2018). Additionally, the highly nonlinear behavior of the structure was evident by the large number of plastic hinges that formed under the selected earthquake records with high intensity.

The NARX neural network is implemented using the neural network toolbox in MATLAB (Mathworks, 2019). In this paper, a tan-sigmoid transfer function in the hidden layer and linear transfer function in the output layer are used. Ground motion acceleration time histories are chosen as input and FE analysis results (i.e. displacement time histories on each floor) are chosen as target values. Bayesian regularization (MacKay, 1992) is adopted as the training algorithm to determine the optimum combination of bias values and weights that minimizes the neural network prediction errors.

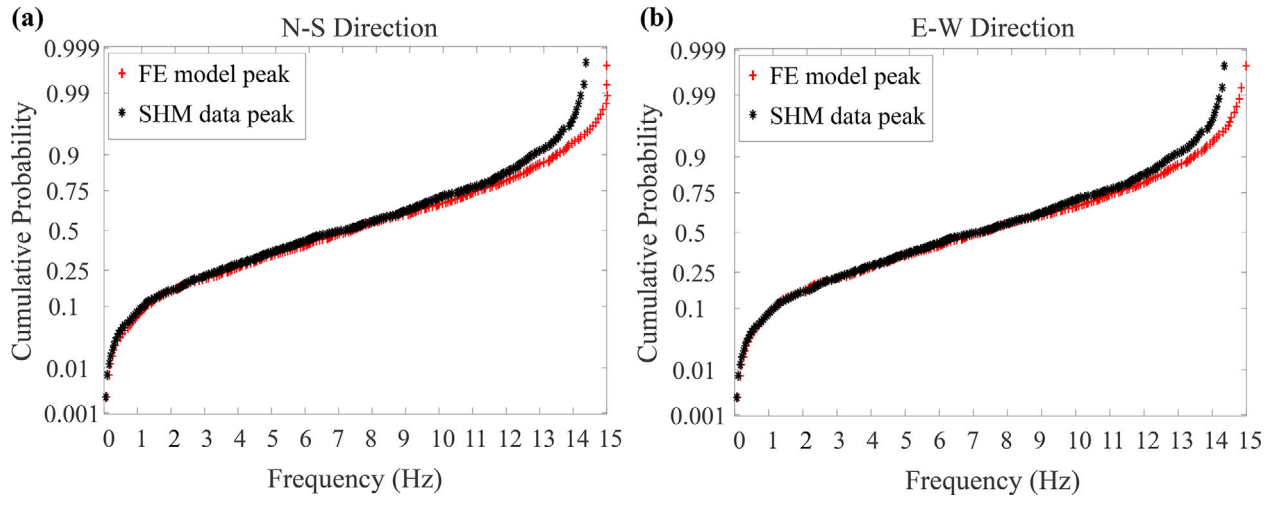


Figure 16. Probability plot comparing occurrence of peaks in PSD ratio for SHM and FE model.

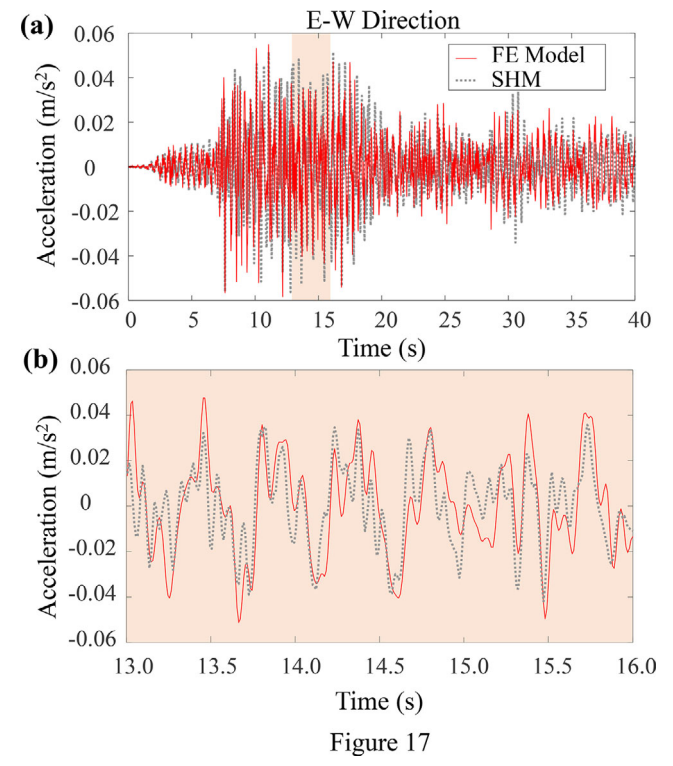


Figure 17. Comparison of acceleration response of the roof obtained from the FE model and SHM data (a) 40 sec. view and (b) 3 sec. view.

A total of 10 ground motion records are used to train the model. NLTHA is conducted for each selected earth-quake using step-by-step direct integration in CSi SAP2000 (CSI, 2018). The selected ground motions and their corresponding displacement time histories are then used to train the NARX neural networks. For training the network, an open loop NARX neural network is used as both input and output data are available during the training phase. The configuration of a neural network is one of the most important aspects that govern its performance. As no significant literature is available for NARX network configuration in nonlinear seismic response prediction applications, a trial network configuration with one hidden layer of 5 neurons and input and feedback delay of 10 is selected.

Accordingly, the network uses 10 points (i.e. 0.05 sec) in the ground motion time series preceding the current time to predict the response at the current time. With this configuration, it was observed that the network was unable to accurately predict the dynamic response. After various systematic trials with different numbers of neurons, a network configuration of 1 hidden layer with 10 neurons is selected. Moreover, the number of input and feedback delays are selected as multiples of the fundamental natural time period of the building. Sensitivity analysis with respect to the delay is conducted to select the optimal delay value.

Figure 18 presents the mean square error with respect to different delay values. As shown, a delay value of 50% of the fundamental natural period significantly reduces the mean square error. Increasing the delay beyond 50% has a lower impact on the mean square error. Since larger delay values increase the training computational time, and in some cases may cause non-convergence, a delay value corresponding to 50% of the fundamental natural period $(T=0.77\,\mathrm{s})$ for both input and feedback is selected in this paper. With this configuration, accurate network performance is observed.

A separate network is trained to predict the response time history of each story. Training data are scaled to range between -1, +1 in order to improve the training efficiency of the model (Zhang et al., 2019). The weights and bias values are adjusted iteratively during the training using the Bayesian regularization back-propagation algorithm (MacKay, 1992) such that the error between the predicted network values and target values reaches a minimum. The MSE, as shown in Equation (6), is taken as the training performance indicator (Arjovsky et al., 2016). Figure 19 shows the variation of MSE with respect to the number of neurons. It can be seen from the figure that adding more neurons after 10 does not decrease the MSE appreciably; hence, 10 neurons are used for training purposes.

Once the networks are trained, they are converted into closed loop configuration to assess their predictive accuracy using another set of earthquakes containing 5 ground motion time series that are not used in training phase.

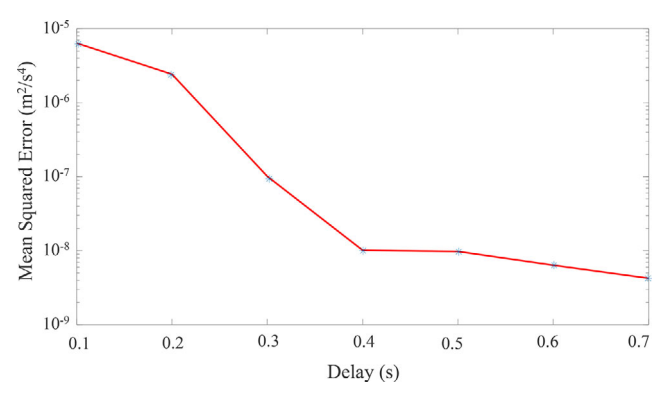


Figure 18. Variation of MSE with delay.

Figures 20 and 21 show the predicted response of the trained neural network for first and roof stories, respectively, under the effect of one of the earthquake signals included in the testing database. As shown, the NARX neural network is capable of predicting the displacement time history with appreciable accuracy. A similar level of prediction accuracy was also observed for the other four earthquake time series of the testing database.

Additionally, a comparison of the predicted displacement time histories in all other stories revealed that the employed NARX configuration with 10 neurons can accurately predict the response of the building under seismic excitation. To further evaluate the accuracy of the trained networks, Figure 22 compares the probability plot of displacement amplitudes obtained using FE analysis to the NARX predictions. The figure compares the FE predicted values obtained for all of the testing data set (i.e. the five testing ground motion signals) to the NARX predicted values. As shown, the NARX network was capable of predicting the displacement with a maximum prediction error of 3% compared to the FE results. It should be noted that other types of ANNs (e.g. feedforward ANNs and LSTM networks) were also trained and tested; however, none of these investigated networks matched the accuracy of the adopted NARX configuration.

Note that given the structural attributes, efficiency of the training algorithm, and the configuration of the adopted neural networks, the number of seismic records required for training can greatly vary. In general, it is essential to define a comprehensive training and testing database that well represents the underlying problem. A larger training database should yield better results; however, given the computational expense associated with direct integration nonlinear finite element analysis, executing the minimum number of FE analysis is preferred. On the other hand, a limited training database can lead to over-fitted models that are not well generalized. The coefficient of determination R² provides an appropriate measure to judge the adequacy of the training dataset (Ouyang, 2017; Tabarsa & Davodi, 2018; Wang, Pedroni, Zentner, & Zio, 2018).

4.4. Incremental dynamic analysis

The trained networks in closed loop configuration are used next to conduct the incremental dynamic analysis. PGA is

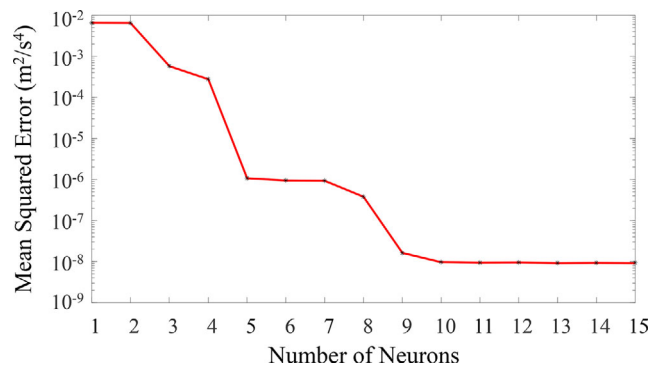


Figure 19. Variation of the MSE with the number of neurons.

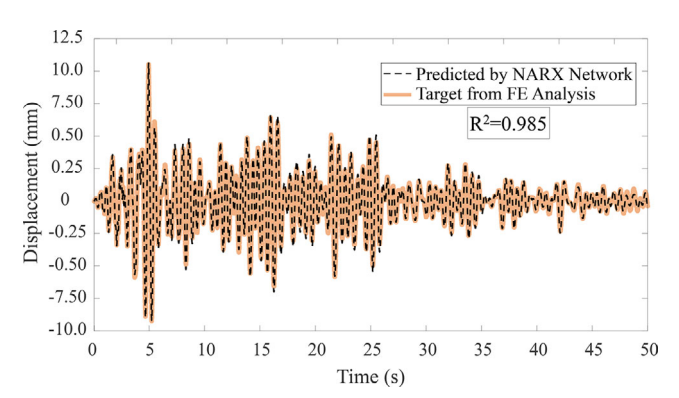


Figure 20. Comparison of displacement response of the first floor predicted using the NARX network and FE analysis.

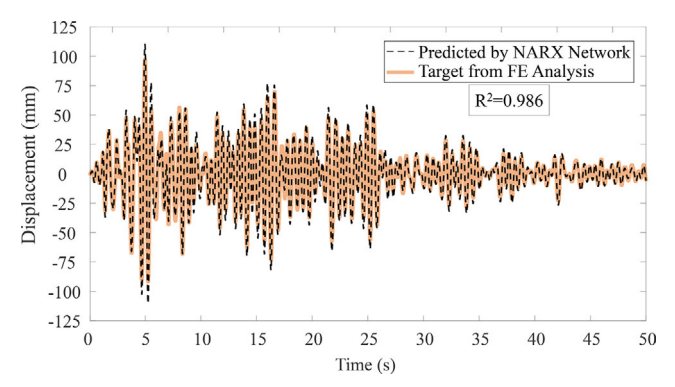


Figure 21. Comparison of displacement response of the roof predicted using the NARX network and FE analysis.

taken as the intensity measure and the IDR is chosen as engineering demand parameter. Fifteen additional ground motions are selected and scaled to cover various levels of PGA, starting from 0.05 g, with 0.05 g increments, until failure. Note that this set of ground motions is not the same one adopted for training and testing the network. Failure is assumed to occur when the maximum IDR reaches or exceeds 3%, which is more than the 2.5% conventional collapse prevention limit (Ibrahim, 2018). Figure 23 shows the profiles of maximum IDR for each earthquake with respect to the story level and the median of the maximum IDR with respect to the story level. It can be seen from this figure that for a given ground motion intensity, the 6th and 7th stories experience relatively higher drifts than others.

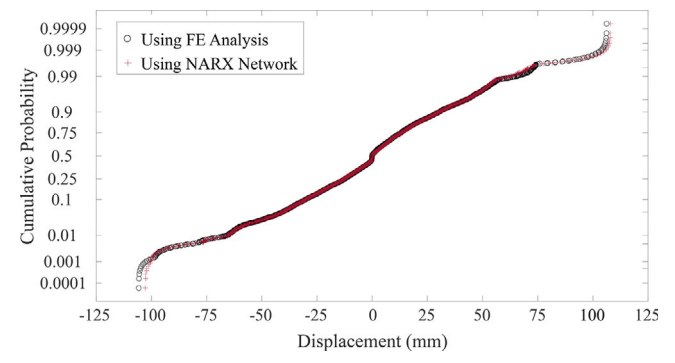


Figure 22. Probability plot of displacement values obtained from the FE analysis versus the NARX prediction.

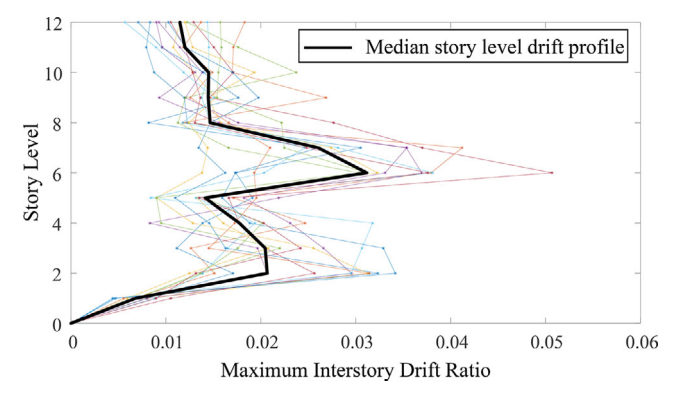


Figure 23. Maximum interstory drift ratio with respect to story level at collapse s.

Figure 24 illustrates the results of IDA for the same additional 15 earthquakes where the response at each story was calculated using the trained NARX neural networks in terms of PGA versus maximum IDR along with the median of the maximum IDR. As shown by the median profile, the maximum IDR increases linearly till PGA of almost 0.6 g, depicting linear behaviour of the building. After a median average value of 0.6 g, softening occurs, signalling the onset of the nonlinear response.

The NARX networks conducted the IDA analysis shown in Figure 24 in approximately five minutes. Conducting nonlinear dynamic analysis for one earthquake using SAP2000 required approximately four hours. This translates to more than 45 days to complete such analysis using traditional nonlinear FE analysis. On the other hand, a total of 15 ground motion records, requiring 60 hours of FE analysis, were used to generate the training and testing database. Additionally, once the NARX networks are trained, a larger number of earthquake records can be easily considered for IDA analysis with nearly no additional computational cost. The analysis has been conducted on a desktop computer with Intel(R) Core (TM) i7-7700 CPU at 3.60 GHz and 16 GB of RAM.

After conducting the IDA, the fragility curves are developed using Equation (3). Figure 25 displays the fragility curve based on the lognormal cumulative distribution function. It can be seen from the figure that the probability of failure (i.e. probability of exceedance of 3% drift ratio limit) is 50% for PGA value of 0.85 g and almost 100% at 1.3 g. Note that recent probabilistic hazard assessments indicate

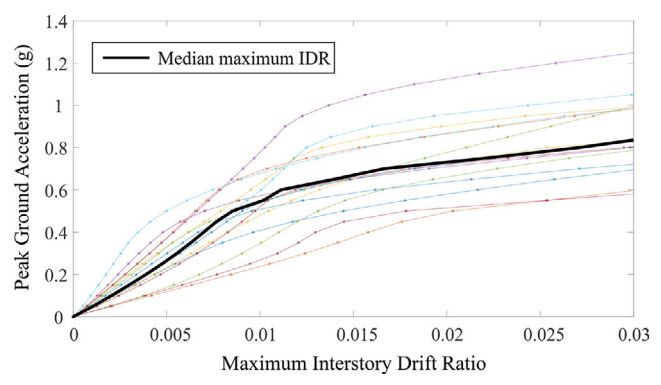


Figure 24. IDA analysis results conducted using NARX networks.

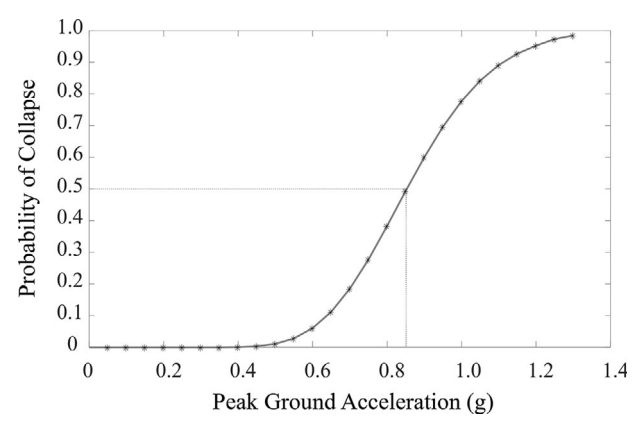


Figure 25. Seismic fragility curve of the investigated building.

that the PGA with 1% probability of being exceeded in the next year is approximately 0.5 g, using the annual peak seismic hazard estimates relevant to seismicity with anthropogenic sources in Oklahoma (Petersen et al., 2018).

5. Conclusions

This paper presented a framework for conducting seismic fragility analysis of multi-story buildings using nonlinear autoregressive exogenous (NARX) input neural networks. The study integrates structural health monitoring data with finite element analysis to calibrate a structural model. A relatively small number of FE simulations, using the calibrated FE model with a range of input ground motions, is used to train and test the NARX networks. The trained networks are then utilized to create response time histories and conduct incremental dynamic analysis. The results of IDA are then used to construct the seismic fragility curves of the building. The presented framework was illustrated on a twelve-story reinforced concrete building. The following conclusion can be drawn:

NARX neural networks are capable of predicting the nonlinear dynamic response of structural systems subjected to seismic excitations. Nevertheless, care should be taken in generating the network training dataset to encompass the range of earthquakes required for the seismic fragility analysis.

- The defined feedback delay in the NARX network has a significant effect on the prediction accuracy. It was found that, for the investigated structure, a delay of approximately 50% of the fundamental time period of the structure, both in input and feedback layers, yields optimum training of the NARX network. Lower feedback delay resulted in loss of accuracy in the results while larger delay required significantly longer training time without considerable gains in prediction accuracy. Sensitivity analysis similar to the one presented in Figure 18 is necessary to establish the optimum value of the feedback delay required to minimize the prediction error.
- The IDA is an important tool in assessing the seismic behaviour of structures. It provides the relationship between the seismic intensity and the corresponding structural response parameter. The IDA curves can be efficiently generated using the proposed framework for a given response parameter. Multiple response parameters can be included in the analysis; however, training time will be affected by the number of required response parameters.
- The proposed framework can efficiently construct the seismic fragility curves of multi-story buildings. Integrating NARX networks and FE analysis to construct the fragility curves led to a significant reduction in the computational time of the fragility analysis. For the investigated case study, the computational time was reduced by approximately 18 times.

Funding

The authors gratefully acknowledge the financial support from the National Science Foundation, Award numbers OAC-1835371 and OAC-1835372.

Acknowledgements

We acknowledge the teams at Scripps Institution of Oceanography and Oklahoma State University that installed the sensors and collected the structural health monitoring data, including Frankie Martinez, Jessie Saunders, Glen Offield, Haejo Kim, Frank Vernon, Juan Reyes Colon, Geoff Davis, Christopher Waite, and Brian Jonson. The research team also acknowledges the support from the residential services, facilities management, and information technology departments at Oklahoma State University for their support in equipment installation and maintenance. The opinions and conclusions presented in this paper are those of the authors and do not necessarily reflect the views of the sponsoring organization.

ORCID

Omid Khandel (i) http://orcid.org/0000-0003-2204-340X Mohamed Soliman http://orcid.org/0000-0003-3160-0933

References

Aghayan, A., Jaiswal, P., & Siahkoohi, H. R. (2016). Seismic denoising using the redundant lifting scheme. Geophysics, 81(3), V249-V260. doi:10.1190/geo2015-0601.1

- Alexandridis, A. (2013). Evolving RBF neural networks for adaptive soft-sensor design. International Journal of Neural Systems, 23(6), 1350029. doi:10.1142/S0129065713500299
- Arjovsky, M., Shah, A., & Bengio, Y. (2016). Unitary evolution recurrent neural networks. Proceedings of the 33rd International Conference on Machine Learning, New York City, New York, USA.
- Baker, J. W. (2015). Efficient analytical fragility function fitting using dynamic structural analysis. Earthquake Spectra, 31(1), 579-599. doi: 10.1193/021113EQS025M
- Celik, O. C., & Ellingwood, B. R. (2009). Seismic risk assessment of gravity load designed reinforced concrete frames subjected to mid-America ground motions. Journal of Structural Engineering, 135(4), 414-424. doi:10.1061/(ASCE)0733-9445(2009)135:4(414)
- CSI. (2018). SAP2000 integrated software for structural analysis and design and reference manual. Computers and Structure Inc., Berkely, CA.
- CSI. (2020). Perform-3D Nonlinear analysis and performance assessment for 3-D structures. User guide. Computers and Structure Inc., Berkely, CA.
- Ellsworth, W. L. (2013). Injection-induced earthquakes. Science (New York, N.Y.), 341(6142), 1225942. doi:10.1126/science.1225942
- Federal Emergency Management Agency. (2000). FEMA 356, Prestandard and commentary for the seismic rehabilitation of buildings. Washington, DC: Federal Emergency Management Agency.
- Gidaris, I., Padgett, J. E., Barbosa, A. R., Chen, S., Cox, D., Webb, B., & Cerato, A. (2017). Multiple-hazard fragility and restoration models of highway bridges for regional risk and resilience assessment in the United States: State-of-the-art review. Journal of Structural Engineering, 143(3), 04016188. doi:10.1061/(ASCE)ST.1943-541X. 0001672
- Gidaris, I., Taflanidis, A. A., & Mavroeidis, G. P. (2015). Kriging metamodeling in seismic risk assessment based on stochastic ground motion models. Earthquake Engineering & Structural Dynamics, 44(14), 2377-2399. doi:10.1002/eqe.2586
- Hilber, H. M., Hughes, T. J., & Taylor, R. L. (1977). Improved numerical dissipation for time integration algorithms in structural dynamics. Earthquake Engineering & Structural Dynamics, 5(3), 283-292. doi:10.1002/eqe.4290050306
- Hurtado, J. E., & Alvarez, D. A. (2001). Neural network-based reliability analysis: A comparative study. Computer Methods in Applied Mechanics and Engineering, 191(1-2), 113-132. doi:10.1016/S0045-7825(01)00248-1
- Ibarra, L. F., & Krawinkler, H. (2005). Global collapse of frame structures under seismic excitations. Technical Report No.152, Blume Earthquake Engineering Center.
- Ibrahim, Y. E. (2018). Seismic risk analysis of multistory reinforced concrete structures in Saudi Arabia. Case Studies in Construction Materials, 9, e00192. doi:10.1016/j.cscm.2018.e00192
- Jaiswal, K. S., Aspinall, W. P., Perkins, D., & Porter, K. A. (2012). Use of expert judgment elicitation to estimate seismic vulnerability of selected building types. Proceedings of 15th World Conference on Earthquake Engineering, Lisbon, Portugal.
- Joghataie, A., & Farrokh, M. (2008). Dynamic analysis of nonlinear frames by Prandtl neural networks. Journal of Engineering Mechanics, 134(11), 961-969. doi:10.1061/(ASCE)0733-9399(2008)134:11(961)
- Joyner, W. B., & Boore, D. M. (1981). Peak horizontal acceleration and velocity from strong motion records including records from the 1979 Imperial Valley, California earthquake. Seismological Society of America, 71(6), 2011-2038.
- Khandel, O., & Soliman, M. (2021). Integrated framework for assessment of time-variant flood fragility of bridges using deep learning neural networks. Journal of Infrastructure Systems, 27(1), 04020045. doi:10.1061/(ASCE)IS.1943-555X.0000587
- Khandel, O., Soliman, M., Floyd, R. W., & Murray, C. D. (2020). Performance assessment of prestressd concrete bridge girders using fiber optic sensors and artificial neural networks. Structure and Infrastructure Engineering.doi:10.1080/15732479.2020.1759658
- Kiani, J., Camp, C., & Pezeshk, S. (2019). On the application of machine learning techniques to derive seismic fragility curves.



- Computers & Structures, 218, 108-122. doi:10.1016/j.compstruc. 2019.03.004
- Lagaros, N. D., & Fragiadakis, M. (2007). Fragility assessment of steel frames using neural networks. Earthquake Spectra, 23(4), 735-752. doi:10.1193/1.2798241
- Lagaros, N. D., & Papadrakakis, M. (2012). Neural network based prediction schemes of the non-linear seismic response of 3D buildings. Advances in Engineering Software, 44(1), 92-115. doi:10.1016/j. advengsoft.2011.05.033
- Lagaros, N. D., Plevris, V., & Papadrakakis, M. (2010). Neurocomputing strategies for solving reliability-robust design optimization problems. Engineering Computations, 27(7), 819-840. doi: 10.1108/02644401011073674
- Lallemant, D., Kiremidjian, A., & Burton, H. (2015). Statistical procedures for developing earthquake damage fragility curves. Earthquake Engineering & Structural Dynamics, 44(9), 1373-1389. doi:10.1002/ eqe.2522
- Lavaei, A., & Lohrasbi, A. (2012). Dynamic analysis of structures using neural networks. Proceedings of 15th World Conference on Earthquake Engineering, Lisbon, Portugal.
- Lin, T., Horne, B. G., Tino, P., & Giles, C. L. (1996). Learning longterm dependencies in NARX recurrent neural networks. IEEE Transaction on Neural Networks, 7, 1329-1338.
- MacKay, D. (1992). A practical Bayesian framework for backpropagation networks. Neural Computation, 4(3), 448-472. doi:10.1162/ neco.1992.4.3.448
- Mander, J. B., Priestley, M. J. N., & Park, R. (1988). Theoretical stressstrain model for confined concrete. Journal of Structural Engineering, 114(8), 1804-1826. doi:10.1061/(ASCE)0733-9445(1988)114:8(1804)
- Masri, S. F., Nakamura, M., Chassiakos, A. G., & Caughey, T. K. (1996). Neural network approach to detection of changes in structural parameters. Journal of Engineering Mechanics, 122(4), 350-360. doi:10.1061/(ASCE)0733-9399(1996)122:4(350)
- Mathworks. (2019). MATLAB: The language of technical computing and user manual. https://www.mathworks.com.
- McNamara, D. E., Rubinstein, J. L., Myers, E., Smoczyk, G., Benz, H. M., Williams, R. A., Hayes, G., Wilson, D., Herrmann, R., McMahon, N. D., Aster, R. C., Bergman, E., Holland, A., & Earle, P. (2015). Efforts to monitor and characterize the recent increasing seismicity in central Oklahoma. The Leading Edge, 34(6), 628-639. doi:10.1190/tle34060628.1
- Menezes Jr., J. M. P., & Barreto, G. A. (2006). A new look at nonlinear time series prediction with NARX recurrent neural network. Proceedings of the Ninth Brazilian Symposium on Neural Networks, Ribeirao Preto, Brazil.
- Moehle, J. P. (2005). Nonlinear analysis for performance-based earthquake engineering. The Structural Design of Tall and Special Buildings, 14(5), 385-400. doi:10.1002/tal.334
- Montana, D. J., & Davis, L. (1989). Training feedforward neural networks using genetic algorithms. Proceedings of the International Joint Conference on Artificial Intelligence, Michigan,
- Newmark, N. M. (1959). A method of computation for structural dynamics. Journal of the Engineering Mechanics Division, 85(3), 67-94. doi:10.1061/JMCEA3.0000098
- Ok, S., Son, W., & Lim, Y. M. (2012). A study of the use of artificial neural networks to estimate dynamic displacements due to dynamic loads in bridges. Proceedings of Journal of Physics: Conference Series, 382-012032, University of Glasgow, Scotland. doi:10.1088/ 1742-6596/382/1/012032
- Otani, S. (1980). Nonlinear dynamic analysis of reinforced concrete building structures. Canadian Journal of Civil Engineering, 7(2), 333-344. doi:10.1139/l80-041
- Ouyang, H. T. (2017). Nonlinear autoregressive neural networks with external inputs for forecasting of typhoon inundation level. Environmental Monitoring and Assessment, 189(8), 376. doi:10.1007/ s10661-017-6100-6
- Pal, S. K., & Mitra, S. (1992). Multilayer perceptron, fuzzy sets, and classification. IEEE Transactions on Neural Networks, 3(5), 683-697. doi:10.1109/72.159058

- Papadrakakis, M., & Lagaros, N. D. (2002). Reliability-based structural optimization using neural networks and Monte Carlo simulation. Computer Methods in Applied Mechanics and Engineering, 191(32), 3491-3507. doi:10.1016/S0045-7825(02)00287-6
- Patra, J. C., & Bornand, C. (2010). Nonlinear dynamic system identification using Legendre neural network. Proceedings of the International Joint Conference on Neural Networks, Barcelona, Spain.
- PEER. (2008). Pacific Earthquake Engineering Research Center (NGA-West2). Berkeley, CA. https://peer.berkeley.edu/ngawest2.
- PEER/ATC-72. (2010). Modeling and acceptance criteria for seismic design and analysis of tall buildings. Applied Technology Council, Redwood, California.
- Petersen, M. D., Mueller, C. S., Moschetti, M. P., Hoover, S. M., Rukstales, K. S., McNamara, D. E., Williams, R. A., Shumway, A. M., Powers, P. M., Earle, P. S., Llenos, A. L., Michael, A. J., Rubinstein, J. L., Norbeck, J. H., & Cochran, E. S. (2018). 2018 One-year seismic hazard forecast for the Central and Eastern United States from induced and natural earthquakes. Seismological Research Letters, 89(3), 1049-1061. doi:10.1785/0220180005
- Rainieri, C., Fabbrocino, G., & Cosenza, E. (2011). Integrated seismic early warning and structural health monitoring of critical civil infrastructures in seismically prone areas. Structural Health Monitoring, 10(3), 291-308. doi:10.1177/1475921710373296
- Rajbhandari, A. M., Anwar, N., & Najam, F. (2017). The use of artificial neural networks (ANN) for preliminary design of high-rise buildings. Proceedings of 6th ECCOMAS Thematic Conference on Computational Methods in Structural Dynamics and Earthquake Engineering, Rhodes Island, Greece.
- Ruiz, L. G. B., Cuellar, M. P., Calvo-Flores, M. D., & Jimenez, M. C. (2016). An application of non-linear autoregressive neural networks to predict energy consumption in public buildings. Energies, 9(9), 684. doi:10.3390/en9090684
- Sabetta, F., Goretti, A., & Lucantoni, A. (1998). Empirical fragility curves from damage surveys and estimated strong ground motion. Proceedings of the 11th European Conference on Earthquake Engineering, Paris, France.
- Salihovic, A., & Ademovic, N. (2017). Nonlinear analysis of reinforced concrete frame under lateral load. Coupled Systems Mechanics, 6(4), 523-537.
- Sarkisian, M., Mathias, N., Garai, R., & Horiuchi, C. (2017). Improving seismic resilience using structural systems with friction-base fuses. Proceedings of the AEI Conference, Oklahoma City, Oklahoma.
- Sheikh, I. A., Khandel, O., Soliman, M., Haase, J. S., & Jaiswal, P. (2019). An integrated framework for seismic risk assessment of reinforced concrete buildings based on structural health monitoring. Proceedings of the IABSE, New York, NY.
- Shokrabadi, M., Banazadeh, M., Shokrabadi, M., & Mellati, A. (2015). Assessment of seismic risks in code conforming reinforced concrete frames. Engineering Structures, 98, 14-28. doi:10.1016/j.engstruct. 2015.03.057
- Sibi, P., Jones, S. A., & Siddarth, P. (2013). Analysis of different activation functions using back propagation neural networks. Journal of Theoretical and Applied Information Technology, 47(3), 1264-1268.
- Siegelmann, H. T., Horne, T., & Giles, C. L. (1997). Computational capabilities of recurrent NARX neural networks. IEEE Transactions on Systems, Man, and Cybernetics, Part B, 27(2), 208-215. doi:10. 1109/3477.558801
- Tabarsa, A., & Davodi, H. (2018). Forecasting nonlinear dynamic response of layered soils due to earthquake motion using artificial neural network. Civil Engineering and Environmental Systems, 35(1-4), 204-222. doi:10.1080/10286608.2019.1590777
- Takeda, T., Sozen, M. A., & Nielsen, N. N. (1970). Reinforced concrete response to simulated earthquakes. Journal of the Structural Division, 96(12), 2557-2573. doi:10.1061/JSDEAG.0002765
- Vamvatsikos, D., & Cornell, C. A. (2002). Incremental dynamic analysis. Earthquake Engineering & Structural Dynamics, 31(3), 491-514. doi:10.1002/eqe.141
- Wang, Z., Pedroni, N., Zentner, I., & Zio, E. (2018). Seismic fragility analysis with artificial neural networks: Application to nuclear



power plant equipment. Engineering Structures, 162, 213-225. doi: 10.1016/j.engstruct.2018.02.024

Wu, R.-T., & Jahanshahi, M. R. (2018). Deep convolutional neural network for structural dynamic response estimation and system identification. Journal of Engineering Mechanics, 145(1), 0401825.

Yi, J. H., Kim, D., Go, S., Kim, J. T., Park, J. H., Feng, M. Q., & Kang, K. S. (2012). Application of structural health monitoring system for reliable seismic performance evaluation of infrastructures. Advances in Structural Engineering, 15(6), 955-967. doi:10.1260/1369-4332.15.6.955

Zain, M., Anwar, N., Najam, F. A., & Mehmood, T. (2017). Seismic fragility assessment of reinforced concrete high-rise buildings using the uncoupled modal response history analysis (UMRHA). Proceedings of International Conference on Earthquake Engineering and Structural Dynamics, Reykjavik, Iceland.

Zhang, R., Chen, Z., Chen, S., Zheng, J., Buyukozturk, O., & Sun, H. (2019). Deep long short-term memory networks for nonlinear structural seismic response prediction. Computers & Structures, 220, 55-68. doi:10.1016/j.compstruc.2019.05.006